Systems & Control Transactions

Research Article - Peer Reviewed Conference Proceeding
ESCAPE 35 - European Symposium on Computer Aided Process Engineering
Ghent, Belgium. 6-9 July 2025
Jan F.M. Van Impe, Grégoire Léonard, Satyajeet S. Bhonsale,
Monika E. Polańska, Filip Logist (Eds.)

PSE PRESS

On Optimisation of Operating Conditions for Maximum Hydrogen Storage in Metal Hydrides

Chizembi Sakulanda[a], Thokozani Majozi[a*]

[a]School of Chemical and Metallurgical Engineering, University of the Witwatersrand, Johannesburg, South Africa
* Corresponding Author: Thokozani.majozi@wits.ac.za

ABSTRACT

The climate crisis continues to grow as an existential threat. Establishing reliable energy resources that are renewable and zero-carbon emitting is a critical endeavour. Hydrogen has emerged as one such critical resource due to its high gravimetric energy density and near-abundant availability. However, it suffers from low volumetric energy density and is incredibly challenging to store and transport. The metal hydride, a solid-state storage method, provides a viable solution to the current limitations. Storage is achieved through the chemical absorption of hydrogen into a porous metal alloy's sublattice. But its challenging thermodynamic functionality leaves a gap between the ideal storage capacity that current industry requires and the limited capacity that reusable metal hydrides currently provide. This work used mathematical modelling to determine optimal operating conditions for a metal hydride in order to maximise hydrogen storage capacity. Computational fluid dynamics is used to simulate the coupled heat and mass transfer that occurs during the absorption process into the metal alloy. The finite volume method is used to discretise governing equations, and the alternating direction implicit method is used for numerical solutions as it proved the most stable platform to conduct analyses. An initial investigation into numerical grid sizing is conducted to determine the optimal node allocation. The impact of the hydride bed thickness and supply pressure are varied and optimised. The alloy $MmNi_{4.6}Al_{0.4}$ is used in the investigation.

Keywords: Metal Hydride, Optimisation, Computational Fluid Dynamics

INTRODUCTION

The climate crisis is an anthropological concern that has had an ever-increasing level of importance in the 21st century. The 2015 Paris Agreement, signed by 196 nations, sought to ideally limit the global temperature increase at 1.5 °C [1]. However, in 2022, the Intergovernmental Panel on Climate Change (IPCC) stated that efforts implemented between its 2022 sitting and the 2015 agreement significantly undershot the targets to reach a 1.5 °C limit [2]. The South African government announced strategies to introduce more renewable power production into its energy sector. However, South Africa is not yet meeting its nationally determined contribution to reach the goal of limiting global warming by 1.5 °C [3].

South Africa has sufficient renewable resources to power a transition to zero-emissions power production, but clean energy integration remains a critical issue. 70% of local project developers working in the renewable energy sector found that the limited physical and institutional capacity to integrate the growing number of renewables into the resource mix are a significant hinderance to the country's transition away from fossil fuels [4].

With its natural abundance and high gravimetric energy density, hydrogen has been positioned as a critical player for 21st century decarbonisation ambitions [5]. Despite its growing attention, there remain some key practical hurdles for the mass adoption of hydrogen. This is due to its low volumetric energy density and difficulty when it comes to storage. An area of growing attention is solid-state storage and that is because it provides a solution to the volumetric energy density shortfall that hydrogen suffers from [6]. The metal hydride is among these solid-state storage solutions.

Background and motivation

Metal hydrides are a very attractive storage pathway for the emerging hydrogen market for several

reasons. The primary is their potential for high storage density. In addition to that, metal hydrides are often recyclable and their formation occurs at safe operational pressures. Once formed, they are also easy to store and can easily by transported [7].

Figure 1 below provides a representation of how the hydrogen molecule approaches the alloy surface and is eventually absorbed into the bulk lattice. The general reaction formula for the formation of a metal hydride where M is the metal, MH is the hydride, x is the hydrogen concentration and Q is the heat released is as follows [8]:

$$M(s) + \frac{x}{2}H_2(g) \leftrightarrow MH_x(g) + Q \quad (1)$$

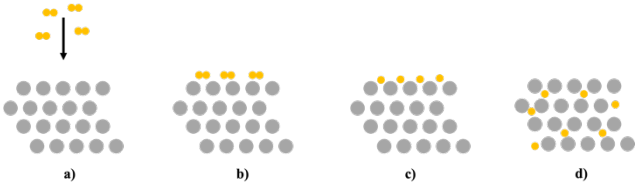

Figure 1. Step-by-step visualisation of hydrogen absoprtion process

Extensive work has gone into mathematically modelling the metal hydride. Understanding the interplay between heat generation and storage capacity is key to ensuring this technology can be adopted into industrial use [9]. Equation 1 shows that heat is a critical component to the hydrogen absorption and desorption cycle, the former being an exothermic reaction and the latter endothermic. A good control of the thermodynamic functions of the metal hydride is critical for reaching any attainable goal of maximising its storage potential.

Therefore, this research aims to develop a two-dimensional model that will accurately simulate a metal hydride system with which an optimisation can be performed.

The prescribed objectives are to:

i. Develop a mathematical model for the heat and mass transfer within the metal hydride reactor using given parameters.
ii. Compare the results of the developed model with existing literature and validate model results.
iii. Investigate the effect of varying particular variables.
iv. Conduct an optimisation on the identified variables.

Literature Review

Metal hydrides can be distinguished into two classifications, interstitial and non-interstitial. The divergence between interstitial and non-interstitial is not drastic but significant enough in that it results in the two classifications having different storage potentials and operating conditions [6]. During the absorption and desorption cycle, very little change occurs to the metal's surface when dealing with an interstitial hydride. The non-interstitial is dependent on the decomposition and recombination of the hydride as a whole. While interstitial hydrides typically have a lower storage density than non-interstitial, they are generally recyclable unlike non-interstitials. It is for this reason that interstitials are perused more commonly in research [6].

Figure 2 shows the general trend across metal hydrides. There is a directly correlative relationship between storage capacity and heat of formation. The lower the storage capacity of a hydride results in a lower the heat of formation and similarly the converse bears true.

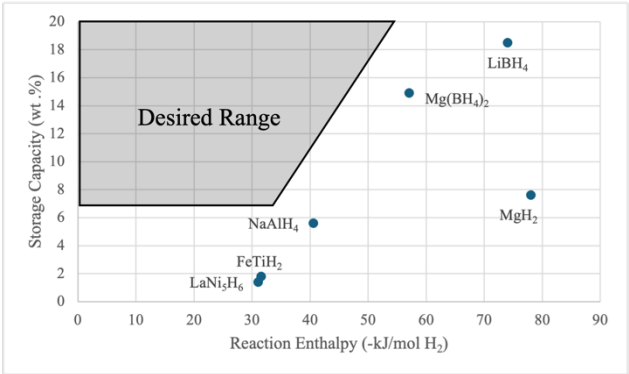

Figure 2. Comparison of different metal hydrides' potential storage density and reaction enthalpies [8]

There is a broad range of metal alloys used to make metal hydrides. Among the many metals and alloys used, a classification of three distinct groups can be formed. These three are intermetallics (Eg. $LaNi_5H_6$), magnesium-based hydrides (Eg. MgH_2) and complex hydrides (Eg. $LiBH_4$, $NaAlH_4$) [7]. The former group is typically interstitial while the latter two groups are often non-interstitial. Some metrics considered when reviewing the classifications are storage capacity, temperature and recyclability. Some conservative estimations suggest that hydrides need only reach a storage capacity of 2 wt.% for stationary applications [10]. Other investigations peg this minimum to be higher with at least 5 wt.% [8]. The US Department of Energy outlines an ultimate gravimetric density target for any hydrogen fuelled light-duty vehicles to be 6.5 wt. % [11].

Unlike complex hydrides and magnesium hydrides, intermetallics have much more suitable operating conditions. In fact, most academic literature models some kind of intermetallic hydride [9]. This is due to their manageable working temperature and pressure ranges, fast kinetics and reusability. However, their benefits are counteracted by their low storage capacity; often, they do not manage to exceed 2 wt.%. Ultimately, their workability supersedes their storage deficiency. The most common alloy that is investigated is the lanthanum penta-nickel

($LaNi_5$) [12]. $LaNi_5$ is often cited for having a high production cost due to the lanthanum. To circumvent this, some investigations use a cheaper rare-earth mischmetal mixture as a replacement for pure lanthanum [19, 20]. This work conducted its investigation with the alloy $MmNi_{4.6}Al_{0.4}$. It is understood that its ideal storage capacity limit resides somewhere between 1 - 1.4 wt.% [13, 14].

MATHEMATICAL MODEL

The absorption/desorption cycle of a metal hydride is a process that involves both heat and mass transfer. It is a two-phase system with the gas phase covering the hydrogen and solid phase covering the hydride bed within the storage vessel. This results in the reactor vessel being a discontinuous medium. However, conservation equations that model heat and mass transfer in a porous medium are intended for a continuous medium. To allow the applicability of these equations, the scale of examination is shifted from microscopic to macroscopic. To do this phase averaging is implemented. This allows the average volume, over which heat and mass transfer takes place, to be larger than the individual bed pores [15].

A standard cylindrical vessel with external cooling is considered – see Figure 3. The heat and mass transfer are modeled in two dimensions, the radial and axial flow. Figure 3 shows two reactor geometries. Figure 3A has hydrogen fed through an axial inlet and its hydride bed occupies the full breadth of the vessel. It is modelled asymmetrically for ease. Figure 3B is an expansion on the axisymmetric condition. The geometry potentially offers a much more even distribution of the hydrogen gas and with it an even generation of heat across the hydride bed [14, 16]. This work makes use of Figure 3B geometry.

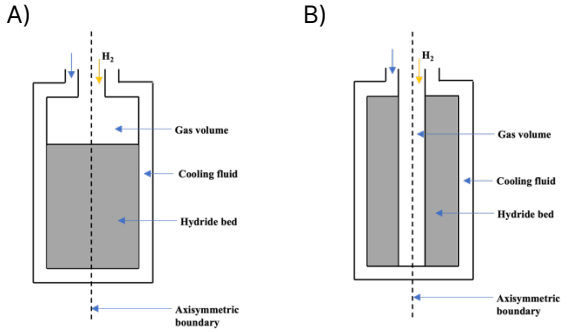

Figure 3. A simple diagram of the two most common reactor geometries

An initial starting point for the thermal governing equation, are the following:

$$\varepsilon\rho_g C_{pg}\frac{\partial T_g}{\partial t} = \frac{1}{r}\frac{\partial}{\partial r}\left(\varepsilon\lambda_{ge} r\frac{\partial T_g}{\partial r}\right) + \frac{\partial}{\partial z}\left(\varepsilon\lambda_{ge}\frac{\partial T_g}{\partial z}\right) - \rho_g C_{pg} v_{gr}\frac{\partial T_g}{\partial r} - \rho_g C_{pg} v_{gz}\frac{\partial T_g}{\partial z} + H_{gs}(T_g - T_s)S - mC_{pg}(T_g - T_s) \quad (2)$$

$$(1-\varepsilon)\rho_s C_{ps}\frac{\partial T_s}{\partial t} = \frac{1}{r}\frac{\partial}{\partial r}\left((1-\varepsilon)\lambda_{se} r\frac{\partial T_s}{\partial r}\right) + \frac{\partial}{\partial z}\left((1-\varepsilon)\lambda_{se}\frac{\partial T_s}{\partial z}\right) + H_{gs}(T_g - T_s)S + m(\Delta H^o + C_{pg}T_g - C_{ps}T_s) \quad (3)$$

Equations 2 and 3 are the thermal balance of the gas and solid phase, respectively [15, 17].

The mathematical formation of the governing equations is established with the following assumptions taken into consideration:

i. The gas phase within the vessel and hydride bed exhibits ideal gas behaviour
ii. The local thermal equilibrium hypothesis is taken to be true
iii. Radiative heat transfer is negligible
iv. Viscous dissipation and compression work are considered negligible
v. Hydride porosity, permeability and heat conductivity remain unchanged during absorption cycle

Of the assumptions, one that provides an immediate simplification to the heat transfer model is the local thermal equilibrium assumption. This allows for the temperature within the gas and solid phase along any radial and axial length at any given time to be the same. This, therefore, eliminates the need for two thermal balances and reduces it down to a single thermal equation:

$$(\rho C_p)_e\frac{\partial T}{\partial t} = \frac{1}{r}\frac{\partial}{\partial r}\left(\lambda_e r\frac{\partial T}{\partial r}\right) + \frac{\partial}{\partial z}\left(\lambda_e\frac{\partial T}{\partial z}\right) - \rho_g C_{pg} v_{gr}\frac{\partial T}{\partial r} - \rho_g C_{pg} v_{gz}\frac{\partial T}{\partial z} + m(\Delta H + T(C_{pg} - C_{ps}) \quad (4)$$

$$(\rho C_p)_e = \varepsilon\rho_g C_{p_g} + (1-\varepsilon)\rho_s C_{p_s} \quad (5)$$

$$\lambda_e = \varepsilon\lambda_{ge} + (1-\varepsilon)\lambda_{se} \quad (6)$$

Another assumption that is commonly used is that of ignoring pressure effects within the vessel and, by extension, ignoring the effect of convective heat transfer. To determine if this assumption is applicable to this investigation, a dimensionless ratio seen in Equation 7 helps identify if the effect of gaseous flow can be neglected or not [18]. If N is found to be much less than 1, then ignoring pressure effects will have a negligible effect on the results of the simulation.

$$N = \frac{\lambda_e \cdot M \cdot L_{gas}^2 \cdot \mu}{\frac{\partial P_{eq}}{\partial T}\cdot\Delta H\cdot\rho_g\cdot K\cdot L_{heat}^2} \quad (7)$$

The continuity equation and reaction kinetics for this system are given by Equations 8 - 12. Equations 8 and 11 are similar in that the former records mass absorption and the latter hydrogenation. There are instances where the thermal equation's heat generation term makes use of the hydrogenation model – see Equation 14. Equation 12 shows a modified van't Hoff equation which accounts for varying hydrogen concentration and hysteresis [9, 14]. The benefit of the model employed in this work is its generality for porous multiphase systems [15]. Its specificity comes in the form of the thermo-physical properties

shown in Table 1.

$$m_{abs} = C_a \exp\left(-\frac{Ea}{RT}\right) \ln\left(\frac{P}{P_{eq}}\right)(\rho_{ss} - \rho_s) \quad (8)$$

$$(1-\varepsilon)\frac{\partial \rho_s}{\partial t} = m_{abs} \quad (9)$$

$$\frac{dx}{dt} = \sigma \frac{(p-p_{eq})}{p_{eq}} \frac{(x-x_f)}{(x_o-x_f)} \exp\left(\frac{-E_a}{RT}\right) \quad (10)$$

$$\varepsilon \frac{\partial \rho_g}{\partial t} + \nabla \cdot \left(\rho_g \underset{v}{\rightarrow}\right) = (\rho_{ss} - \rho_s)(1-\varepsilon)\frac{dx}{dt} \quad (11)$$

$$lnP_{eq} = \frac{\Delta H}{R_g T} - \frac{\Delta S}{R_g} + (\emptyset \pm \varphi) tan\left[\pi\left(\frac{\left(\frac{H}{M}\right)}{\left(\frac{H}{M}\right)} - \frac{1}{2}\right)\right] \pm \frac{\beta}{2} \quad (12)$$

The following are the boundary conditions used:
Reactor axis

$$\frac{\partial T}{\partial r}(z, 0, t) = 0 \quad (13a)$$

Reactor base

$$-\lambda_e \frac{\partial T}{\partial z}(H, r, t) = h\big(T(H, r, t) - T_f\big) \quad (13b)$$

Reactor lateral area

$$-\lambda_e \frac{\partial T}{\partial r}(z, R, t) = h\big(T(z, R, t) - T_f\big) \quad (13c)$$

Table 1: Alloy and hydrogen thermo-physical properties [15, 18]

Alloy properties	
Density (kg/m^3), ρ_s	8400
Specific heat (J/kg.K), C_{ps}	419
Effective thermal conductivity (W/m.K), λ_e	1.6
Porosity, ε	0.5
Effective saturated density (kg/m^3), ρ_{ss}	4259
Effective initial density (kg/m^3), ρ_s	4200
Activation energy (J/kg.K), E_a	21170
Entropy (J/mol H_2.K), ΔS	107.2
Enthalpy (J/mol H_2), ΔH	28000
Hydrogen properties	
Thermal conductivity (W/m.K), λ_{ge}	0.127
Specific heat (J/kg.K), C_{pg}	14183
Density (kg/m^3), ρ_g	0.084
Molar mass (kg/mol), M_{H_2}	2x10^{-3}
Dynamic viscosity (Pa.s), μ	8.9x10^{-6}
Constants	
Gas constant (J/mol.K), R	8.314
Reaction constant (s^{-1}), σ	75
Slope factor, $\emptyset$	0.35
Constant, φ	0.15
Hysteresis factor, β	0.2

NUMERICAL METHOD

A critical component of computational fluid dynamic work is the discretisation technique used to solve the governing equations. Initially, this work sought an exploration of the possibilities between the finite difference method (FDM) and finite volume method (FVM) [19, 20]. In literature, there are diverging paths with many opting for FVM and few opting for FDM [8]. This work settled on using node-centred FVM. MATLAB was the chosen software to conduct the work.

The conductive terms after the FVM treatment can be seen in Equation 14. Note the hydrogenation modified heat generation term.

$$(\rho C_p)_e \frac{\partial T}{\partial t} = \frac{1}{r_P}\left(r_E \lambda_e \frac{T_E - T_P}{r_E - r_p} - r_W \lambda_e \frac{T_P - T_W}{r_P - r_E}\right) + \left(\lambda_e \frac{T_N - T_P}{Z_N - Z_p} - \lambda_e \frac{T_P - T_S}{Z_P - Z_S}\right) + \frac{\Delta\rho \cdot (1-\varepsilon)\Delta H}{M_{H_2}} \frac{dx}{dt} \quad (14)$$

In addition to the discretisation method, there is a need to select a solution technique for solving these governing equations. On this matter, there is typically one of two ways that can be selected – explicit solutions or implicit solutions. This investigation sought to determine the most beneficial option between using explicit and implicit solution methods [19-21]. The solution which provided the best numerical stability was the implicit solution, specifically the alternating-direction implicit (ADI) method. The application of this is shown in Equation 15 and 16. A tridiagonal matrix algorithm is then utilised. The Dirichlet boundary condition is directly applied, and the Robin boundary conditions are treated with a difference approximation [19, 22].

Radial step:

$$(\rho C_p)_e \frac{T_{i,j}^{n+1/2} - T_{i,j}^{n}}{\Delta t/2} = \frac{1}{r_P}\left(r_E \lambda_e \frac{T_E^{n+1/2} - T_P^{n+1/2}}{r_E - r_p} - r_W \lambda_e \frac{T_P^{n+1/2} - T_E^{n+1/2}}{r_P - r_E}\right) + \left(\lambda_e \frac{T_N^{n} - T_P^{n}}{Z_N - Z_p} - \lambda_e \frac{T_P^{n} - T_S^{n}}{Z_P - Z_S}\right) + Q \quad (15)$$

Axial step:

$$(\rho C_p)_e \frac{T_{i,j}^{n+1} - T_{i,j}^{n+1/2}}{\Delta t/2} = \left(\lambda_e \frac{T_N^{n+1} - T_P^{n+1} + 1}{Z_N - Z_p} - \lambda_e \frac{T_P^{n+1} - T_S^{n+1}}{Z_P - Z_S}\right) + \frac{1}{r_P}\left(r_E \lambda_e \frac{T_E^{n+1/2} - T_P^{n+1/2}}{r_E - r_p} - r_W \lambda_e \frac{T_P^{n+1/2} - T_E^{n+1/2}}{r_P - r_E}\right) + Q \quad (16)$$

RESULTS

Using the criterion of Equation 7, it was determined that it is suitable for this work to neglect the effect of gaseous flow and neglect convective heat transfer.

An appreciable baseline figure to remember for comparison is an estimation on how much hydrogen would be stored in a high-pressure (350 bar) gas vessel without a packed hydride bed. At a volume of 8.41x10^{-5} m^3, radius of 7.5x10^{-3} m and length of 4.75x10^{-1} m, and with the aid of the ideal gas equation, an estimated 2.39x10^{-3} kg can be stored in such a vessel. A vessel of steel composition would result in a storage capacity

somewhere in the region of 0.6 wt.%. A lighter composite of aluminium and carbon fibre, as is increasingly used [23], would raise this to a potential capacity of 0.8 wt.%

Grid sizing

Before testing the effect of operating conditions, an important consideration is the effect of the numerical grid size used for the simulation. A base 20x200 grid is initially selected. An investigation into varying the gride size across a predetermined range of values was conducted. The adjustment of the radial resolution has a more prominent impact than the axial resolution variation. Figure 3 below shows how increasing nodal points in both the axial and radial direction increases storage capacity. This is understandable as coarser numerical grids often lead to higher inaccuracies.

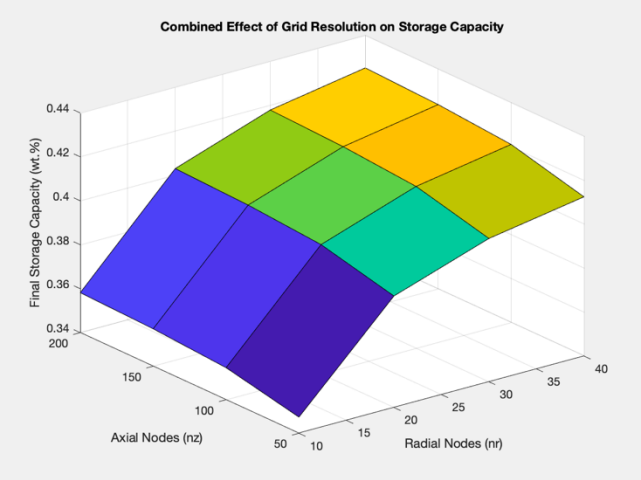

Figure 3. 3D plot of the effect of axial and radial nodes numbering on storage capacity

A preliminary optimisation run saw that the Δstorage convergence threshold of 0.5% change was reached at a 270x1295 grid size and yielded 0.448 wt.% capacity.

Supply pressure and bed thickness

Supply pressure plays a critical role in the attempt to maximise storage. Equation 10 shows how the difference between the P and P_{eq} is a driving force for absorption. Like the grid sizing, pressure was varied across a predetermined range. Table 2 shows that larger supply pressures allow for more hydrogen to be absorbed. The optimisation simulation found convergence at 43.2 bar with a storage of 0.411 wt.%.

In addition to supply pressure, this investigation tested the reactor bed thickness. Something helpful to consider is the surface area/volume ratio. An increased radius increases the required surface area across which the hydrogen must diffuse. Increasing the diffusion area increases the diffusion resistance and ultimately limits the amount absorbed – see Table 3. An optimisation was also run for bed thickness, but the convergence criterion was not met. However, the plotting did indicate that a maximum storage of just over 0.4 wt.% was reached between 0.005m and 0.01m.

Table 2: Varied supply pressure and the impact on storage capacity

Pressure (bar)	Wt.%
5	0.016
10	0.096
15	0.186
20	0.270
25	0.337
30	0.390

Table 3: Varied bed thickness and the impact on storage capacity

Radius (m)	Wt.%
$5x10^{-3}$	0.390
$75x10^{-3}$	0.169
$10x10^{-2}$	0.092
$15x10^{-2}$	0.037

CONCLUSIONS

The metal hydride is a promising hydrogen storage pathway. The developed heat and mass transfer modelled for this investigation, simulated on the $MmNi_{4.6}Al_{0.4}$ alloy, yielded stable and comparable results to that seen in literature. The peak storage capacity values achieved in this work, while just under half of what is understood to be the ideal threshold, were appreciable enough for this investigation. It is also lower than the comparably sized high-pressure gas storage vessel.

The intention to store hydrogen at safe and operable pressures which will aid its transportation and storage characteristics remains a significant hurdle to overcome. The metal hydride, at least the intermetallic kind, is still not yet a fully viable route but its promise remains alive. This work produced valuable insight into the effect that numerical grid sizing, supply pressure and bed thickness have on gas absorption for hydride operating.

ACKNOWLEDGEMENTS

Thank you to the National Research Foundation for funding this work (UID47440).

REFERENCES

1. United Nations Climate Change. The Paris Agreement. [Online] Available at: https://unfccc.int/process-and-meetings/the-paris-agreement/the-paris-agreement.

2. United Nations. UN climate report: It's 'now or never to limit global warming to 1.5 degrees. [Online] Available at: https://news.un.org/en/story/2022/04/1115452.
3. Climate Transparency & Energy Systems Research Group. Climate Transparency Report: Comparing G20 Climate Action, Climate Transparency. University of Cape Town (2022)
4. Renaud, C., Tyler, D. E., Roff, A. & Steyn, D. G. Accelerating renewable energy industrialisation in South Africa: What's stopping us? *Meridian Economics* (2020).
5. Barretoa, L., Makihiraa, A. & Riahi, K. The hydrogen economy in the 21st century: a sustainable development scenario. *International Journal of Hydrogen Energy* 28:267-284 (2003).
6. Chen, Zhen; Ma, Zhongliang; Zheng, Jie; Li, Xingguo; Akiba, Etsuo & Li, Hai-Wen. Perspectives and challenges of hydrogen storage in solid-state hydrides. *Chinese Journal of Chemical Engineering* 29:1-12 (2021).
7. Sakintuna, B., Lamari-Darkrimb, F. & Hirscher, M. Metal hydride materials for solid hydrogen storage: A review. *International Journal of Hydrogen Energy* 32:1121-1140 (2007).
8. Dornheim, M. Thermodynamics of Metal Hydrides: Tailoring Reaction Enthalpies of Hydrogen Storage Materials. In: Thermodynamics - Interaction Studies - Solids, Liquids and Gases. Ed.J. C. Moreno-Pirajan. Intechopen (2011)
9. Mohammadshahi, S., Gray, E. & Webb, C. A review of mathematical modelling of metal hydride systems for hydrogen storage applications. *International Journal of Hydrogen Energy* 41:3470-3484 (2016).
10. Modi, P. & Aguey-Zinsou, K.-F. Room Temperature Metal Hydrides for Station and Heat Storage Applications: A Review. *Frontiers in Energy Research* 9:616115 (2021).
11. Office of Energy Efficiency & Renewable Energy. DOE Technical Targets for Onboard Hydrogen Storage for Light-Duty Vehicles. [Online] Available at: https://www.energy.gov/eere/fuelcells/doe-technical-targets-onboard-hydrogen-storage-light-duty-vehicles
12. Rusman, N. & Dahari, M. A review on the current progress of metal hydrides material for solid-state hydrogen storage applications. *International Journal of Hydrogen Energy* 41:12108-12126 (2016.).
13. Singh, R. K., Gupta, B. K., Lototsky, M. & Srivastava, O. On the synthesis and hydrogenation behaviour of MmNi5−xFex alloys and computer simulation of their P–C–T curves *Journal of Alloys and Compounds*. 373:208-213 (2004).
14. Muthukumar, P., Madhavakrishna, U. & Dewan, A. Parametric studies on a metal hydride based hydrogen storage device. *International Journal of Hydrogen* 32:4988-4997 (2007).
15. Whitaker, S. Simultaneous Heat, Mass, and Momentum Transfer in Porous Media: A Theory of Drying. In: Advances in Heat Transfer. Ed. J. P. Hartnett & T. F. I. Jr. Academic Press, INC (1977).
16. Hasnain, M., Sezer, H. & Mason, J. H. Modeling heat and mass transfer in metal hydride hydrogen storage systems: Impact of operating parameters and reactor geometry. *International Journal of Hydrogen* 71:1045-1055 (2024).
17. Ben Nasrallah, S., Jemni, A. Heat and Mass Transfer Model in Metal-Hydride Reactors. *International Journal of Hydrogen Energy* 22:67-76 (1997).
18. Chaise, A., Marty, P., Rango, P. d. & Fruchart, D. A simple criterion for estimating the effect of pressure gradients on hydrogen absorption in a hydride reactor. *International Journal of Heat and Mass Transfer* 52:4564-4572 (2009).
19. Patankar, S. V. Numerical Heat Transfer and Fluid Flow. Hemisphere Publishing Corporation/McGraw-Hill Book Company (1980)
20. Ozisik, M. N., Orlande, H. R., Colaco, M. J. & Cotta, R. M. Finite Difference Methods in Heat Transfer. CRC Press 2017
21. Roache, P. J. Computational Fluid Dynamics Hermosa Publishers (1972)
22. Smith, G. H. Numerical Solution of Partial Differential Equations: Finite Difference Methods. Oxford University Press (1985).
23. Xu, Y., Zhou, Y., Li, Y. & Ding, Z. Research Progress and Application Prospects of Solid-State Hydrogen Storage Technology. *Molecules* 29:1767 (2024).